Science of the Total Environment 579 (2017) 82–92

Contents lists available at ScienceDirect

Science of the Total Environment

journal homepage: www.elsevier.com/locate/scitotenv

# Spatiotemporal patterns of paddy rice croplands in China and India from 2000 to 2015

Geli Zhang [a], Xiangming Xiao [a,b,*], Chandrashekhar M. Biradar [c], Jinwei Dong [a], Yuanwei Qin [a], Michael A. Menarguez [a], Yuting Zhou [a], Yao Zhang [a], Cui Jin [a], Jie Wang [a], Russell B. Doughty [a], Mingjun Ding [d], Berrien Moore III [e]

[a] Department of Microbiology and Plant Biology, and Center for Spatial Analysis, University of Oklahoma, Norman, OK 73019, USA
[b] Ministry of Education Key Laboratory for Biodiversity Science and Ecological Engineering, Institute of Biodiversity Sciences, Fudan University, Shanghai, 200438, China
[c] International Center for Agricultural Research in Dry Areas, Amman, 11195, Jordan
[d] Key Lab of Poyang Lake Wetland and Watershed Research of Ministry of Education and School of Geography and Environment, Jiangxi Normal University, Nanchang, 330022, China
[e] College of Atmospheric and Geographic Sciences, University of Oklahoma, Norman, OK, 73019, USA

## HIGHLIGHTS

- Annual paddy rice maps in China and India were generated for first time using MODIS data.
- Spatiotemporal patterns of paddy rice fields were analyzed in China and India during 2000–2015.
- Paddy rice area decreased by 18% in China but increased by 19% in India.
- Paddy rice area shifted northeastward in China while widespread expansion detected in India.

## GRAPHICAL ABSTRACT

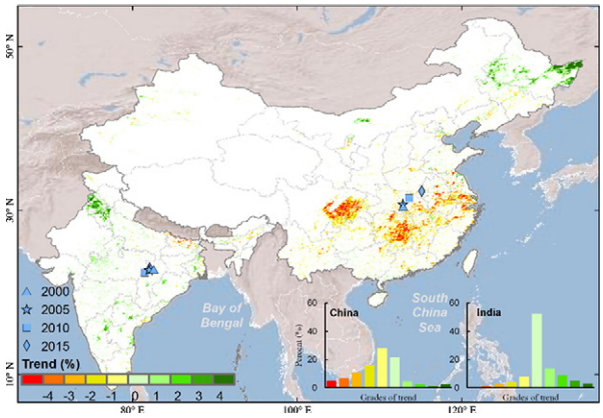


Paddy rice croplands underwent a significant decrease in South China and increase in Northeast China from 2000 to 2015, while paddy rice fields expansion is remarkable in northern India. The paddy rice fields centroid in China moved northward due to the substantial rice planting area shrink in Yangtze River Basin and rice area expansion in high latitude regions (e.g., Sanjiang Plain).

## ARTICLE INFO

*Article history:*
Received 28 August 2016
Received in revised form 29 October 2016
Accepted 30 October 2016
Available online 17 November 2016

Editor: Jay Gan

*Keywords:*
Paddy rice agriculture

## ABSTRACT

Due to rapid population growth and urbanization, paddy rice agriculture is experiencing substantial changes in the spatiotemporal pattern of planting areas in the two most populous countries—China and India—where food security is always the primary concern. However, there is no spatially explicit and continuous rice-planting information in either country. This knowledge gap clearly hinders our ability to understand the effects of spatial paddy rice area dynamics on the environment, such as food and water security, climate change, and zoonotic infectious disease transmission. To resolve this problem, we first generated annual maps of paddy rice planting areas for both countries from 2000 to 2015, which are derived from time series Moderate Resolution Imaging Spectroradiometer (MODIS) data and the phenology- and pixel-based rice mapping platform (RICE-MODIS), and analyzed the spatiotemporal pattern of paddy rice dynamics in the two countries. We found that China

* Corresponding author at: 101 David L. Boren Blvd., Norman, OK 73019, USA.
*E-mail address:* xiangming.xiao@ou.edu (X. Xiao).

http://dx.doi.org/10.1016/j.scitotenv.2016.10.223

China
India
MODIS
Food security
Phenology-based algorithm

experienced a general decrease in paddy rice planting area with a rate of 0.72 million (*m*) ha/yr from 2000 to 2015, while a significant increase at a rate of 0.27 *m* ha/yr for the same time period happened in India. The spatial pattern of paddy rice agriculture in China shifted northeastward significantly, due to simultaneous expansions in paddy rice planting areas in northeastern China and contractions in southern China. India showed an expansion of paddy rice areas across the entire country, particularly in the northwestern region of the Indo-Gangetic Plain located in north India and the central and south plateau of India. In general, there has been a northwesterly shift in the spatial pattern of paddy rice agriculture in India. These changes in the spatiotemporal patterns of paddy rice planting area have raised new concerns on how the shift may affect national food security and environmental issues relevant to water, climate, and biodiversity.



## 1. Introduction

Rice feeds more than half of the human population in the world (Kuenzer and Knauer, 2013). >90% of rice production is from Asia (Maclean and Hettel, 2002). China and India have the largest rice planting areas, the most grain production, and the highest amount of rice consumption in the world. Paddy rice agriculture in these two countries plays a pivotal role for both national and global food security. In addition to food security, rice paddy is related to a number of environmental and human health issues. For example, paddy rice field management regimes affect greenhouse gas (methane) emission and climatic warming (Chen et al., 2013; Li et al., 2003; Sass and Cicerone, 2002; van Groenigen et al., 2013), as well as water use and water resource security (Kuenzer and Knauer, 2013; Samad et al., 1992). Paddy rice agriculture was also found to be related to zoonotic infectious disease transmission, as rice paddies are an important habitat for wild birds and domestic poultry (Gilbert et al., 2014; Gilbert et al., 2008). Therefore, it is important to track the spatiotemporal changes in land use of paddy rice agricultural areas in these two countries.

Several efforts have been taken to document the spatial extent of paddy rice agriculture in China and India (Frolking et al., 2006; Gumma et al., 2015; Liu et al., 2014b; Xiao et al., 2005). In China, previous efforts to map paddy rice fields include: 1) combining a remote sensing-based land cover map for croplands type and agricultural census data (rice area and management) (Frolking et al., 2002); 2) land cover datasets in circa 5-year epochs including paddy rice category by using Landsat imagery and a visual interpretation approach (Liu et al., 2005; Liu et al., 2010); 3) simulation of paddy rice area based on the Spatial Production Allocation Model (SPAM), land distribution, administrative unit census of crop data, agricultural irrigation data, and crop suitability data (Liu et al., 2013; Liu et al., 2014b); and 4) paddy rice mapping through temporal profile analysis of time series MODIS data (Sun et al., 2009; Xiao et al., 2005). In India, the studies about paddy rice field mapping include the district-level rice cropping maps by combining a series of census data sets of rice cropping (Frolking et al., 2006), and MODIS-based paddy rice mapping (Gumma et al., 2011; Xiao et al., 2006). None of the aforementioned projects have generated annual maps of paddy rice agriculture in these two countries, and comparative analyses of spatiotemporal patterns of paddy rice fields between these two countries have not yet been conducted.

Considering the fact that no spatially explicit maps are available for understanding the spatiotemporal dynamics of paddy rice agriculture in these two largest rice-production countries, it is a priority to apply a robust method for national scale monitoring of paddy rice fields. Earlier studies used traditional classifiers such as supervised (e.g., Maximum Likelihood Classification) or unsupervised classifiers and single/multiple images for paddy rice mapping. However, these approaches are dependent on image statistics, training sample collection, and/or human visual interpretation, and may produce more uncertainties when transferring these methods to other regions or periods. Recent studies increasingly use the phenological characteristics of paddy rice in the flooding and transplanting phase to extract the location of paddy rice fields (Sakamoto et al., 2009; Shi et al., 2013; Sun et al., 2009; Xiao et al., 2006; Xiao et al., 2005), which is based on the discovery that the flooding/transplanting signals can be detected by using the relationship between the Land Surface Water Index (LSWI) and Normalized Difference Vegetation Index (NDVI), or Enhanced Vegetation Index (EVI) (Xiao et al., 2002b). This algorithm has recently been used for paddy rice mapping at regional or national scales, including in China (Sun et al., 2009; Xiao et al., 2005; Zhang et al., 2015), the Mekong Basin (Kontgis et al., 2015; Sakamoto et al., 2009), South Asia (Xiao et al., 2006), and the major rice growing countries of Asia (Nelson and Gumma, 2015). In these efforts, some improvements over the original algorithm have been made, including pre-determining the temporal window of transplanting phase by using land surface temperature (Zhang et al., 2015) or agricultural phenology observation (Sun et al., 2009), and modified threshold values in the formula (LSWI + 0.05 ≥ EVI or NDVI) when detecting flooding and transplanting signals for paddy rice fields (Sakamoto et al., 2009).

Although this phenology-based classification strategy has been widely used for paddy rice mapping, previous studies have not utilized the method to continuously monitor paddy rice fields at the national scale, because bad observation (clouds, cloud shadows, snow, aerosols, etc.) ratios and data availability to capture vegetation phenology are variable across large regions. The ability to continuously monitor paddy rice fields is particularly important for the tropical regions in China and India where a cyclic, monsoonal climate causes persistent cloud cover during rainy season (Kontgis et al., 2015). Although Synthetic Aperture Radar (SAR) imaging has advantages, such as not being affected by clouds or solar illumination, the SAR-based approach has not been used for large-scale paddy rice mapping due to the limited availability of SAR data (Bouvet et al., 2009; Dong et al., 2006; Miyaoka et al., 2013; Nelson et al., 2014; Wu et al., 2011; Yang et al., 2008).

In order to better understand the recent paddy rice agriculture dynamics in China and India, the objective of this study is two-fold: 1) to map annual paddy rice planting area for China and India from 2000 to 2015 using time series MODIS data and a phenology-based rice algorithm, and 2) to investigate the spatiotemporal changes in paddy rice fields in both countries from the perspectives of location, climate, and elevation. To our limited knowledge, this study provides the first picture of spatiotemporal changes in paddy rice fields for the two most populous countries. The resultant paddy rice maps are expected to serve land use management and planning, food security policy making, climate change monitoring, water resource usage, and other applications.

## 2. Data and methods

### 2.1. Study area

Paddy rice is generally distributed within the monsoon areas of China and India. In China, the continental monsoon climate can be classified as subtropical in the south and temperate in the north. Precipitation mostly falls in summer season, but with significant moisture gradients from southeast to northwest. Due to the temperature difference in northern and southern China, paddy rice monoculture occurs

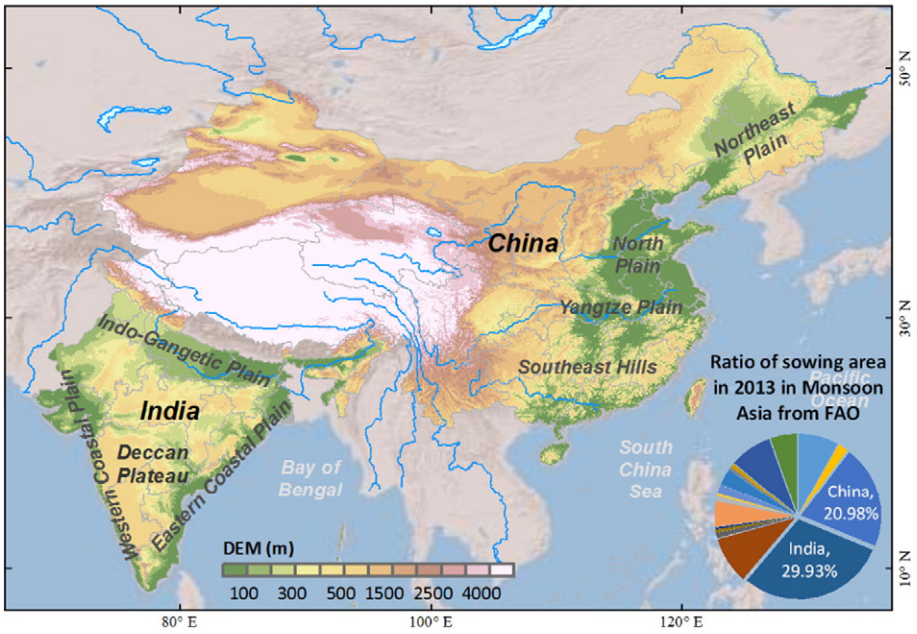


**Fig. 1.** The location of the study area (China and India) and its digital elevation model (DEM). The inset in the figure is the ratios of sowing areas of paddy rice in China and India to that in Monsoon Asia in 2013. The data of sowing area of paddy rice in different countries is from FAOSTAT (http://faostat.fao.org/). The administrative boundaries in China and India are acquired from the GADM (http://www.gadm.org/). The DEM is from Shuttle Radar Topography Mission (SRTM) 90 m Digital Elevation Database, obtained from https://lta.cr.usgs.gov/SRTM.

in northern China and paddy rice polyculture occurs in southern China. Both climate and complex topography affect the vertical and horizontal distributions of paddy rice, which is mainly distributed in the alluvial plains and river basins along China's major rivers and coastal areas in eastern China (Fig. 1).

In India, climate ranges from tropical in the south to temperate and alpine (Himalayas) in the north, and includes four climatic types: tropical wet, tropical dry, subtropical humid, and montane. The tropical monsoon dominates India's annual climate, which can be divided into rainy season (June–October), dry season (March–May), and cool season (November–February). The annual monsoon plays a critical role in planting paddy rice as a polyculture across the country. In terms of topography, the terrain in most parts of India is low and smooth, which is suitable for planting paddy rice. Paddy rice is widely distributed in the Indo-Gangetic alluvial plain, especially in northern India (Fig. 1).

### 2.2. Data and preprocessing

#### 2.2.1. MODIS data and processing

Time series vegetation index (VI) data and land surface temperature (LST) data were used in this study. The VIs were calculated using the 8-day composite surface reflectance products (MOD09A1) (Vermote and Vermeulen, 1999), acquired from the Land Processes Distributed Active Archive Center (https://lpdaac.usgs.gov/). Standard MODIS products are organized in a tile system using a sinusoidal projection, and each tile covers an area of 1200 km × 1200 km (approximately 10 latitude by 10 longitude at the equator). A total of 24 tiles (H25-26V03, H23-27V04, H23-28V05, H24-29V06, H24-26V07, H28V07, and H25V08) from 2000 to 2015, including 17,496 images, were used for China and India. The MODIS data was used to calculate four VIs, including NDVI, EVI (Huete et al., 2002), LSWI (Xiao et al., 2002a; Xiao et al., 2002b), and Normalized Difference Snow Index (NDSI) (Hall et al., 1995; Hall et al., 2002) (Eq. (1)–(4)). Then we identified clouds by using both the data quality layer in the MOD09A1 products and an additional restriction with a blue reflectance of ≥0.2 (Xiao et al., 2005). Snow is identified by a widely used approach (NDSI >0.40 and NIR > 0.11) (Hall et al., 1995; Hall et al., 2002). The observations identified as cloud or snow were excluded from analyses of land cover types and transplanting/flooding signals of paddy rice fields.

$$NDVI = \frac{\rho_{nir} - \rho_{red}}{\rho_{nir} + \rho_{red}} \quad (1)$$

$$EVI = 2.5 \times \frac{\rho_{nir} - \rho_{red}}{\rho_{nir} + 6 \times \rho_{red} - 7.5 \times \rho_{blue} + 1} \quad (2)$$

$$LSWI = \frac{\rho_{nir} - \rho_{swir}}{\rho_{nir} + \rho_{swir}} \quad (3)$$

$$NDSI = \frac{\rho_{green} - \rho_{nir}}{\rho_{green} + \rho_{nir}} \quad (4)$$

where $\rho_{blue}$, $\rho_{green}$, $\rho_{red}$, $\rho_{nir}$, and $\rho_{swir}$ are the surface reflectance for the blue, green, red, near-infrared, and shortwave-infrared bands, respectively.

Minimum daily temperature was used to determine the thermal growing season in this study. MODIS has two Land Surface Temperature (LST) products available at 1-km resolution, MOD11A2 from the Terra satellite (local time ~10:30 AM and ~22:30 PM) and MYD11A2 from the Aqua satellite (~13:30 PM and ~01:30 AM). The observations at ~01:30 AM (from the Aqua satellite) have the lowest temperatures, and are close to the minimum daily temperature (Zhang et al., 2015). Thus, we used the Aqua-derived MYD11A2 data in this study. The gaps in time series LST data due to bad-quality observations were also gap-filled by using the linear interpolation approach. Then the first and last dates of stable temperatures larger than 5 °C in continuous three 8-day intervals were extracted as the start and end dates of the thermal growing season. The resultant maps of the start and end dates of thermal growing season were resampled to 500 m using the nearest neighbor method to match the vegetation index maps. The resultant maps of thermal growing season in 2003 were used to identify paddy rice fields from 2000 to 2002, due to the unavailability of MYD11A2 data in 2000–2002.

Land cover information from the MODIS Land Cover product (MCD12Q1) with 500 m resolution was also used as non-rice masks. Specifically, permanent wetland derived from MCD12Q1 (according to

IGBP classification system) was used as the wetland mask. The MCD12Q1 data were only available from 2001 to 2012, so we used 2001 data to fill the gaps in 2000, and 2012 data to fill the gaps in 2013–2015.

#### 2.2.2. Other datasets

The National Land Cover Dataset (NLCD) of China at a 1-km spatial resolution, obtained from the Data Center for Resource and Environmental Sciences of the Chinese Academy of Sciences (http://www.resdc.cn/), was generated through visual interpretation and digitization of Landsat Thematic Mapper (TM) and Enhanced Thematic Mapper (ETM+) images acquired over multiple periods (1980s, 1995, 2000, 2005, 2008, and 2010) (Liu et al., 2014a; Liu et al., 2005). It includes six primary land cover categories and 25 subtypes. The overall accuracy of the 25 subclasses was above 91.2% (Liu et al., 2014a). The paddy rice layers of 2000, 2005, 2008, and 2010 NLCD datasets were used for comparison in this study. The wetland map derived from NLCD of China in 2010 was used as a supplementary wetland mask for 2000–2015 to exclude natural wetlands in China, which was resampled to 500 m based on the nearest neighbor method to match the vegetation index data from MOD09A1.

The International Rice Research Institute (IRRI) recently released a rice map of six countries in South Asia during 2000–2001 (http://irri.org/our-work/research/policy-and-markets/mapping/remote-sensing-derived-rice-maps-and-related-publications). This map was also derived from MOD09A1 product between June 2000 and May 2001, which are based on the spectral matching techniques, decision trees, and ideal temporal profile data banks. Here it is referred to as IRRI-Rice map, which has 12 rice classes, including the irrigated and rainfed rice (Gumma et al., 2011). The overall accuracy of IRRI-Rice map was 80% for all classes. The irrigated rice layer in the IRRI-Rice map during 2000–2001 in India was used for comparison in this study.

The agricultural census data, which were derived from 2000 to 2014 statistical yearbooks of China (http://www.stats.gov.cn/tjsj/) and 2000–2006 statistical reports of India (http://indiastat.com), were used to compare and evaluate the MODIS-based paddy rice maps at the provincial level. The sowing area of rice in India from 2000 to 2014, derived from FAOSTAT (http://faostat.fao.org/), was used to evaluate the changes in MODIS-based paddy rice fields in India.

### 2.3. Methods

#### 2.3.1. Improved algorithm to identify flooding and transplanting of paddy rice fields

The flooding signals in rice transplanting phase are critical features to identify paddy rice fields, as paddy rice is the sole crop type to be transplanted and to grow in water-soil mixture fields. Through temporal profile analysis of remote sensing data, Xiao et al. (2002b) found that the mixture of rice plants and water (open canopy) during transplanting phases can be tracked by the relationship between the vegetation greenness index (NDVI or EVI) and the water index (LSWI), simply by using the equation: LSWI + 0.05 ≥ EVI or LSWI + 0.05 ≥ NDVI. This simple algorithm was first applied to map paddy rice in South Asia, Southeast Asia and southern China (Xiao et al., 2006; Xiao et al., 2005), and then extended to national scale rice mapping efforts in China and Bangladesh (Gumma et al., 2014; Sun et al., 2009). The application of the algorithm in temperate regions was also proven to be effective by using MODIS or Landsat images (Dong et al., 2015; Jin et al., 2015; Qin et al., 2015; Wang et al., 2015; Zhang et al., 2015).

We recently improved the implementation of the algorithm by incorporating the temperature-based time window for rice transplanting, which was derived from MODIS LST data (Dong et al., 2016; Qin et al., 2015; Zhang et al., 2015; Zhou et al., 2016). Rice plants are not transplanted until air temperature reaches a threshold, so that plants will not suffer damages from low temperatures. In our previous study, we determined that the likely start and end dates of flooding and transplanting (SOF and EOF for short) for paddy rice is the start and end dates of nighttime LST remaining above 5 °C (LST 5 °C, for short), respectively (Zhang et al., 2015). In this study, for the region with monoculture in the northern part of study area (Fig. S1), including Heilongjiang, Jilin, Liaoning, and Inner Mongolia provinces in China, we redefined the EOF as the date of start date of LST 5 °C (Fig. S2a) plus 80 days in order to explicitly extract suitable period for flooding and transplanting in this region. The determination of EOF in northern part of study area will help to identify paddy rice area and remove some disturbances and noises, e.g., summer flooding in August. For the southern part of study area, the end date of LST 5 °C was considered as EOF (Fig. S2b). The temperature-based time window of flooding and transplanting also helps remove the false flooding signals from snow or snowmelt in temperate regions and the mountainous regions (Zhang et al., 2015). The improved algorithm was applied to identify paddy rice fields in temperate and cold temperate zones such as northeastern China (Zhang et al., 2015).

In this study, we applied the improved algorithm to China and India over the period of 2000–2015 for the flooded paddy rice. Note that the rain-fed paddy rice was not included in this specific study due to the unavailability of flooding signals. The EVI and LSWI within the time window of flooding and transplanting were used to identify the observations with signals of flooding and transplanting considering that EVI is more sensitive than NDVI to show the flooding signals of paddy rice (Zhang et al., 2015), and a pixel is assumed to be a "potential or likely" paddy rice field if one or more observations were identified in that manner (Eq. (5)–(8)).

$$F_{Ti} = \begin{cases} 1 & (\mathrm{LSWI}_{Ti} + 0.05 \geq \mathrm{EVI}_{Ti}) \\ 0 & (\mathrm{LSWI}_{Ti} + 0.05 < \mathrm{EVI}_{Ti}) \end{cases} \quad (5)$$

$$Rice_p = \mathrm{Max}(F_{T1}, F_{T2}, \ldots, F_{Tn})(SOF \leq T \leq EOF) \quad (6)$$

$$SOF = DOY(\text{start date of } LST_{\text{night}} \geq 5\,^{\circ}\mathrm{C}) \quad (7)$$

$$EOF = \begin{cases} DOY(\text{start date of } LST_{\text{night}} \geq 5\,^{\circ}\mathrm{C}) + 80 \text{ (north region)} \\ DOY(\text{end date of } LST_{\text{night}} \geq 5\,^{\circ}\mathrm{C}) \text{ (south region)} \end{cases} \quad (8)$$

where *Ti* is the 8-day composite period in the order of *i* between *SOF* and *EOF*, $F_T$ is the flooding area in the 8-day composite at *T* between the *SOF* and *EOF*, and $Rice_p$ is the potential paddy rice area before masking non-rice land cover layers.

#### 2.3.2. Regional implementation of the paddy rice mapping algorithm

In order to take advantage of recent progress in land cover mapping and to reduce commission errors in paddy rice maps, we used several non-cropland data products as mask layers (Xiao et al., 2005, 2006; Zhang et al., 2015). First, we generated maps of evergreen vegetation from analysis of LSWI time series data (Xiao et al., 2009; Xiao et al., 2002c; Xiao et al., 2005). If LSWI value of a pixel is larger or equal to 0.15 in all good observations in one year, it is labeled as evergreen vegetation. We generated annual evergreen vegetation maps, and then a 15-year evergreen vegetation frequency map. In order to reduce the error due to effects of data quality on evergreen vegetation mapping, evergreen vegetation can be identified if it had at least seven detections in 15 years (2000–2014, ~50% detection rate). Second, we used the PALSAR-based forest map in 2010 at 50 m spatial resolution (Qin et al., 2016), which was resampled to 500 m using the nearest neighbor method to be spatially consistent with the vegetation index maps from MOD09A1. Third, we generated maps of sparse vegetation (e.g., saline and alkaline land, build-up) using the annual maximum EVI <0.4 (Zhang et al., 2015). Fourth, we used available maps of natural wetlands: NLCD-based wetland in 2010 in China (Liu et al., 2005) and IGBP-based wetland from MOD12Q1 from 2001 to 2012. Fifth, we used Shuttle Radar Topography Mission (SRTM) 90 m Digital Elevation

Database to generate a digital elevation model (DEM) mask in order to remove the disturbance from low lying area flooding located in mountain region, which is the region above 2600 m above sea level (*asl.*) (Nelson and Gumma, 2015) or with a slope >4°. Last, the length of LST 5 °C (Fig. S2c) <100 days was used as a temperate-based mask throughout the study area, which can help to remove the noise occurring in cold region or montane areas. After excluding land cover by using these masks, annual paddy rice maps were generated (Fig. S3).

Accuracy assessment of land cover maps is a critical component in the production of land cover maps. In order to assess the accuracy of annual paddy rice maps in both countries from 2000 to 2015, we conducted an inter-comparison with existing national/regional paddy rice maps and agricultural census data. The existing paddy rice data we have collected include: 1) NLCD in China in ca. 2000, 2005, 2008, and 2010 (Liu et al., 2005; Liu et al., 2010; Liu et al., 2013); and 2) the IRRI-based paddy rice map during 2000–2001 in India (Gumma et al., 2011). Abundant ground-based survey validations have been conducted in our previous regional studies, including northern China (Zhang et al., 2015), southern China (Xiao et al., 2005), central China (Wang et al., 2015), and India (Biradar and Xiao, 2011). These validations generally covered most paddy rice fields in these two countries in certain years. Given the huge land areas in both China and India and limited resources (financial and human), it is challenging and beyond our capacity to collect national level ground survey data for both countries. Therefore, in this paper, we focus on the inter-comparison among the data products available to the public. Furthermore, we will release the data and conduct a crowd-sourcing validation approach in an online data portal in the future.

#### 2.3.3. Characterizing spatial pattern of paddy rice planting area trends

To investigate the spatial and temporal pattern changes of paddy rice in China and India, we aggregated binary paddy rice maps into fractional rice maps within a block (window) of 10 × 10 pixels (~5-km spatial resolution) and calculated a spatially explicit map of the linear trend of paddy rice fields expansion. Based on the resultant map of paddy rice area change rates from 2000 to 2015 at ~5-km spatial resolution, we investigated where significant changes in paddy rice area took place in China and India. The slope of linear trend was calculated with the following formula:

$$Slope = \frac{n \times \sum_{i=1}^{n}(i \times A_i) - \sum_{i=1}^{n} i \sum_{i=1}^{n} A_i}{n \times \sum_{i=1}^{n} i^2 - \left(\sum_{i=1}^{n} i\right)^2} \quad (9)$$

where *slope* is the change rate of paddy rice area; $i$ is the order of year from 1 to $n$, and $n$ is the number of years; $A_i$ is the area percentage of paddy rice fields of year $i$. If *slope* > 0, then paddy rice area increased. If *slope* < 0, then paddy rice area decreased, and if *slope* = 0, there was no change.

In addition, we employed the centroid movement model by identifying the centroids and shifts of paddy rice fields in these two countries to analyze the spatial and temporal changes in paddy rice area (Zuo et al., 2014). The location of centroids for a given time $t$ could be calculated using the equations below:

$$X(t) = \frac{\sum_{i=1}^{m}(A_i(t) \times X_i(t))}{A(t)}, Y(t) = \frac{\sum_{i=1}^{m}(A_i(t) \times Y_i(t))}{A(t)} \quad (10)$$

where $X(t)$ and $Y(t)$ are the longitude and latitude coordinates of centroid of paddy rice in year $t$. $A_i(t)$ is the area of paddy rice in province $i$; $m$ is the total number of provinces in each country; $X_i(t)$ and $Y_i(t)$ represent the longitude and latitude coordinates of paddy rice in province $i$.

## 3. Results

### 3.1. Inter-comparison of paddy rice maps from multiple sources

Comparisons with existing land use maps showed the reliability of the paddy rice maps in this study. In China, the Landsat-based NLCD datasets agreed well with the MODIS-based paddy rice maps in 2000, 2005, 2008, and 2010. The spatial distribution of MODIS-based paddy rice fields were consistent with those of the NLCD-based paddy rice fractional layers in each of the four time periods, particularly for the pixels with paddy rice area percentage ≥ 40% (Fig. 2a, b, Fig. S4). The comparison of provincial and prefectural area estimates between MODIS-based and NLCD-based maps was significantly correlated at both provincial ($R^2$ ranging from 0.84–0.89) and prefectural levels ($R^2$ ranging from 0.72–0.77) (Fig. 2e, f, Fig. S4). The slopes were close to 1, and the RMSE ranged from $4.7 \times 10^3$ km$^2$ to $6.2 \times 10^3$ km$^2$ at the provincial level and from $0.84 \times 10^3$ km$^2$ to $0.98 \times 10^3$ km$^2$ at the prefectural level (Fig. 2e, f, Fig. S4).

In India, the spatial pattern of MODIS-based paddy rice fields in 2000–2001 was closely consistent with that of IRRI-based product (Fig. 2c, d), with $R^2$ equal to 0.92 and 0.69 at the provincial level and prefectural level, respectively, and with RMSE equal to $4.80 \times 10^3$ km$^2$ and $0.47 \times 10^3$ km$^2$ at the provincial level and prefectural level, respectively (Fig. 2g, h). Both slopes were close to 1 (Fig. 2g, h).

Furthermore, we also compared MODIS-based paddy rice area with agricultural census data of China and India at provincial level (Fig. S5). These comparisons showed high consistency between them; $R^2$ ranged from 0.77–0.92 in China and 0.79–0.81 in India. Finally, we also compared the variations in paddy rice area between MODIS-based results and FAOSTAT in India. We found high consistency of variations between them in India (correlation coefficient equal to 0.83 during 2002–2014, $P < 0.001$, Fig. S6). The higher area estimate of FAOSTAT could be related to the data set's inclusion of rain-fed rice area in India.

Generally, the MODIS-based products had high consistency with the existing local and periodic paddy rice maps in both spatial patterns and magnitudes. Also, the comparisons between MODIS-based paddy rice area and agricultural census data showed high consistency between them. Therefore, the new paddy rice products were reliable for tracking paddy rice agriculture dynamics in both countries. We included the MODIS-based paddy rice area estimates at the province level for India and China. For more information, please refer to the Table S1 in *SI*.

### 3.2. Geographical characteristics of paddy rice distribution in China and India

The paddy rice planting area in 2015 in China and India is 33.04 and 29.02 m ha, respectively (Fig. 3). Paddy rice fields in China is mostly distributed in the alluvial plains in the east of China with an average elevation <400 m, including northeast China and southeast China (Fig. 4, Figs. S7, S8). In northeast China, paddy rice is located in the Northeast Plain with a latitude range of 45–48°N and a longitude range of 130–134°E (Fig. 4, Figs. S7, S8). The distribution of paddy rice fields show a dendritic shape alongside the rivers. In the southeast China, paddy rice is mainly concentrated in the south of North Plain, Yangtze Plain, and Sichuan Basin, with a latitude range of 25–33°N and a longitude range of 103–122°E (Fig. 4, Figs. S7, S8). There is also some paddy rice fields sporadically distributed in the terraced fields of the southeast hills and Yunnan–Guizhou Plateau. Paddy rice of India is widely spread all over the country, except for the Thar Desert in the northwestern part of India (Fig. 4, Fig. S7). Areas with the high density of paddy rice fields are located in the Indo-Gangetic Plain in the north of India, with a latitude range of 20–32°N and a longitude range of 74–88°E, and the Eastern Coastal Plain in the east coast of India, with a latitude range of 8–20°N (Fig. 4, Figs. S7, S8). In central India, paddy rice fields are sporadically distributed (Fig. 4, Fig. S7).

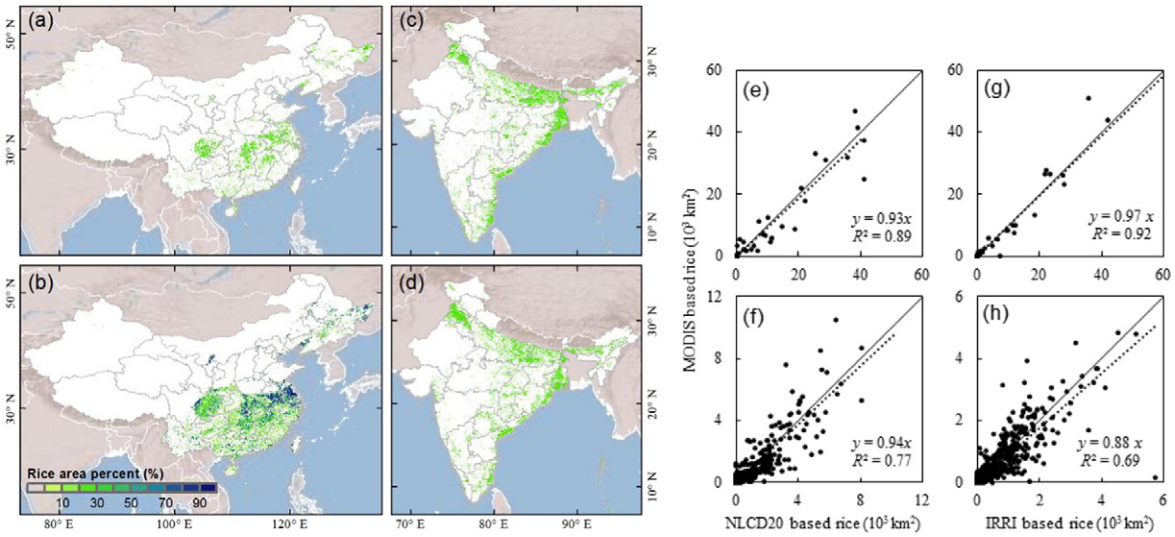


**Fig. 2.** The comparison of MODIS-based paddy rice maps with the existing paddy rice maps. (a) and (c) are the MODIS-based paddy rice maps in China of 2010 and in India of 2000–2001, respectively. (b) is the National Land Cover Dataset (NLCD)-based paddy rice map in China of 2010. (d) is the International Rice Research Institute (IRRI)-based paddy rice map (Gumma et al., 2011) in India of 2000–2001. (e) and (f) are the scatter plots for the comparisons between MODIS-based and NLCD-based paddy rice at provincial and prefectural level in China of 2010, respectively. (g) and (h) are the scatter plots for the comparison between MODIS-based and IRRI-based paddy rice at provincial and prefectural level in India of 2000–2001, respectively.

In terms of climate zones (Figs. S8, S9), paddy rice in China is concentrated in the temperate region, including Cfa climate (Temperate, without dry season and hot summer), Cwa climate (Temperate, dry winter and hot summer), and Dwa climate (Cold, dry winter and hot summer). Paddy rice in India is mainly distributed in the temperate and tropical regions, including Cwa climate, Aw climate (Tropical and savannah), and Bsh climate (Arid, steppe and hot) (Figs. S8, S9). In terms of elevation zones, paddy rice fields in China and India are mainly concentrated in the region with elevation <400 m (Fig. S8).

### 3.3. Characterizing spatial pattern of paddy rice planting area trends in China and India

The inter-annual distribution of paddy rice fields differed between China and India from 2000 to 2015. China had a decreased paddy rice planting area with a rate of 0.72 *m* ha/yr, while planting area increased significantly at a rate of 0.27 *m* ha/yr in India (Fig. 3). Paddy rice planting area in China had a substantial decrease of ~18% from 40.1 × $10^6$ ha in 2000, to 33.0 × $10^6$ ha in 2015. The paddy rice area increased first, reached the maximum (about 45.9 × $10^6$ ha) in 2006, then gradually declined from 2006 to 2015. India had a stable and moderate increase in planting area of 19%, from 24.5 × $10^6$ ha in 2000 to 29.0 × $10^6$ ha in 2015. It is important to point out that the difference in paddy rice planting area between China and India became smaller, from 15.6 × $10^6$ ha in 2000 to 4.0 × $10^6$ ha in 2015 (Fig. 3).

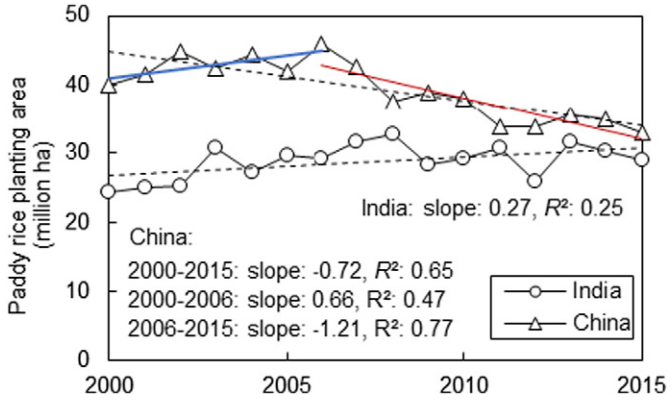


**Fig. 3.** Variations of MODIS-based paddy rice croplands in China and India from 2000 to 2015.

In China, the areas with significant changes in paddy rice area ($P < 0.05$ and $|r| > 1\%$) accounted for 50.2% of all the rice gridcells (Fig. 5), approximately an 11.1% increase ($r > 1\%$) and a 39.1% decrease ($r < -1\%$) in paddy rice area (Table S2). The change in the spatial distribution of paddy rice fields showed an evident increase in northern China and a decrease in southern China. Significant loss of paddy rice area ($P < 0.05$ and $r \leq -1\%$) occurred in the Yangtze Plain in southeast China along a latitude range of 25–33°N and a longitude range of 100–120°E (Figs. 5, 6a, b), including Hunan, Sichuan, Jiangxi, Anhui, Chongqing, Jiangsu, Zhejiang, and Hubei provinces. These regions accounted for 86% of the total significant decrease in paddy rice area in China. Significant expansion of paddy rice areas ($P < 0.05$ and $r \geq 1\%$) occurred in northeast China along a latitude range of 45–48°N and a longitude range of 120–134°E (Figs. 5, 6a, b), and was mainly located in Sanjiang Plain in Heilongjiang province. These regions accounted for ~66% of significant increase in paddy rice area in China, followed by Inner Mongolia, Jilin, and Jiangsu. The increase in paddy rice area in the high-latitude regions led to a northeastward shift of the national paddy rice area centroid in China (Fig. 5). In terms of climate zones, the region with significant increase in paddy rice area are located in the cold zones (Dwa and Dwb), and those with significant decrease in paddy rice area are mainly distributed in the temperate zones (Cfa, Cfb, Cwa, and Cwb) (Fig. 6d, Fig. S9), which further illustrated the northward shift of the national rice area centroid in China. In terms of elevation zones, the regions with a significant decrease in paddy rice area were dominated in the region with the elevation range of 300–500 m, due to the low-lying hills in southeast China where the main regions with significant decrease in paddy rice area were located (Fig. 6c).

In India, expansion of paddy rice fields occurred all over the country (Fig. 5), and the regions with statistically significant changes in paddy rice area ($P < 0.05$ and $|r| > 1\%$) accounted for 39.3% of all the rice gridcells; approximately 30.7% of the area increased and 8.6% decreased (Table S2). Significant expansion of paddy rice fields occurred in the northwest of Indo-Gangetic Plain in north India with a latitude range of 28–32°N (Figs. 5, 6a), followed in the central and south plateau of India, including Punjab, Haryana, Karnataka, and Andhra Pradesh (larger than 8% of the significant increasing region ($P < 0.05$ and $r \geq 1\%$)).

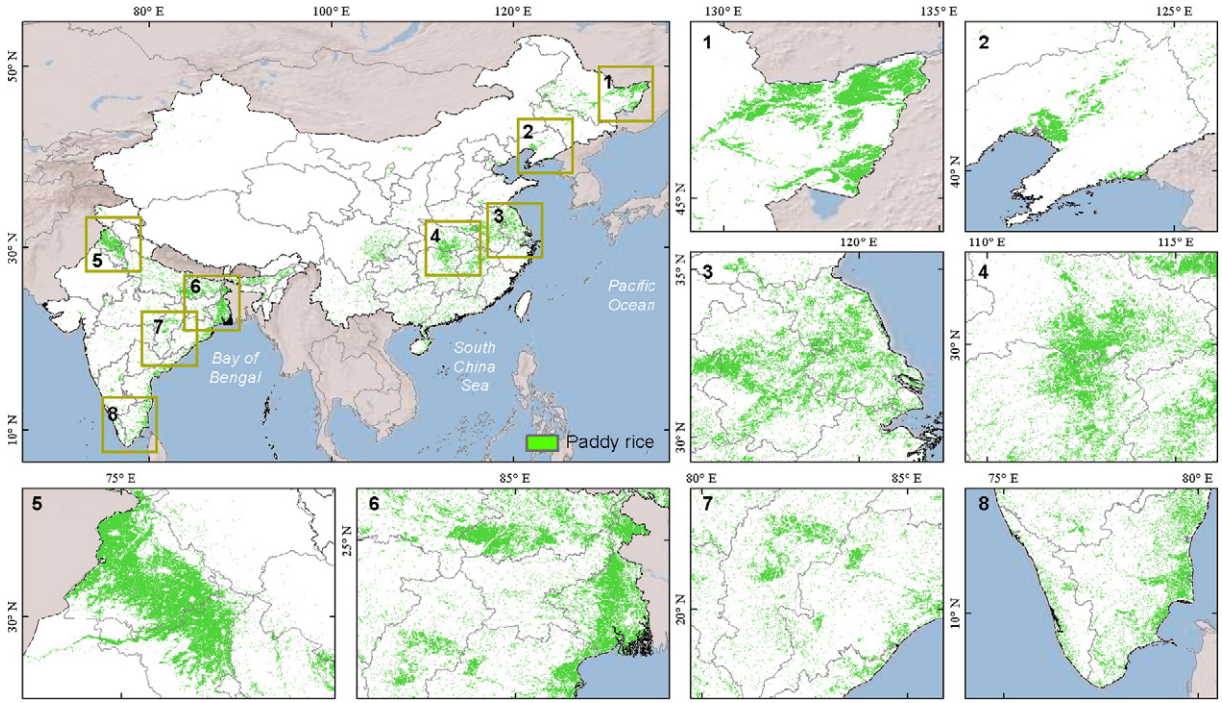


**Fig. 4.** Spatial distribution of paddy rice croplands in China and India in 2015. The figures in the right and bottom are the zoom-in figures.

Significant loss of paddy rice area occurred sporadically over small regions, for example, on the east of Indo-Gangetic Plain of north India with a longitude range of 91–96°E (Figs. 5, 6b), including Bihar, Assam, and West Bengal (larger than 10% of the significant decreasing region ($P < 0.05$ and $r \leq -1\%$)). The changes in spatial pattern of paddy rice planting areas resulted in the centroid shift from east to west and north in India (Fig. 5). In terms of climate zones, paddy rice fields in arid (BWh and BSh) and temperate (Csa, Csb, Cwa) zones increased (Fig. 6d, Fig. S9). In terms of elevation zones, paddy rice fields showed significant increase in all the elevation zones, especially with the elevation range of 200–300 m (Fig. 6c).

## 4. Discussion

### *4.1. From cropland mapping to paddy rice mapping at moderate spatial resolution*

Over the past few decades, land cover mapping at the global scale has aggregated all cropland types into a single category, for example, in cropland of the MCD12Q1 products from MODIS images (Friedl et al., 2010), cropland of the GlobCover product from the MEdium Resolution Imaging Spectrometer (MERIS) (Arino et al., 2008), and the Landsat-based global cropland extent from the FROM-GC datasets

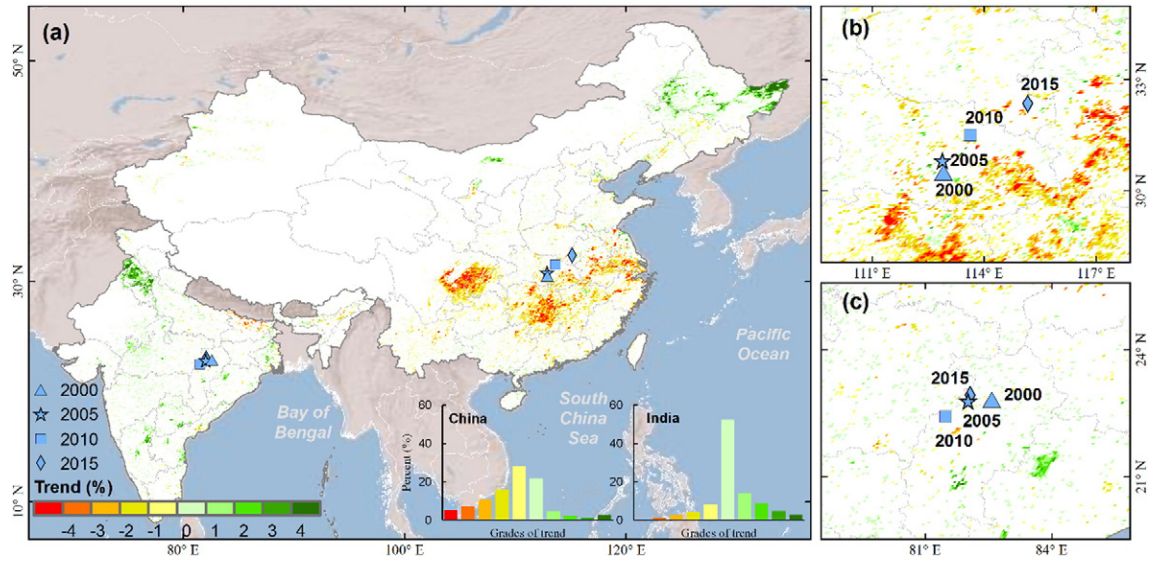


**Fig. 5.** Geographical pattern of the paddy rice change rates. a) Spatial distribution of the significant paddy rice trend ($P < 0.05$) at 5 × 5 km gridcells, the insets show the distributions of different paddy rice change rate levels in China and India. The trajectory of paddy rice centroid from 2000 to 2015 is shown in the map a. (b) and (c) are the zoom-in figures for the trajectories of paddy rice centroid in China and India, respectively.

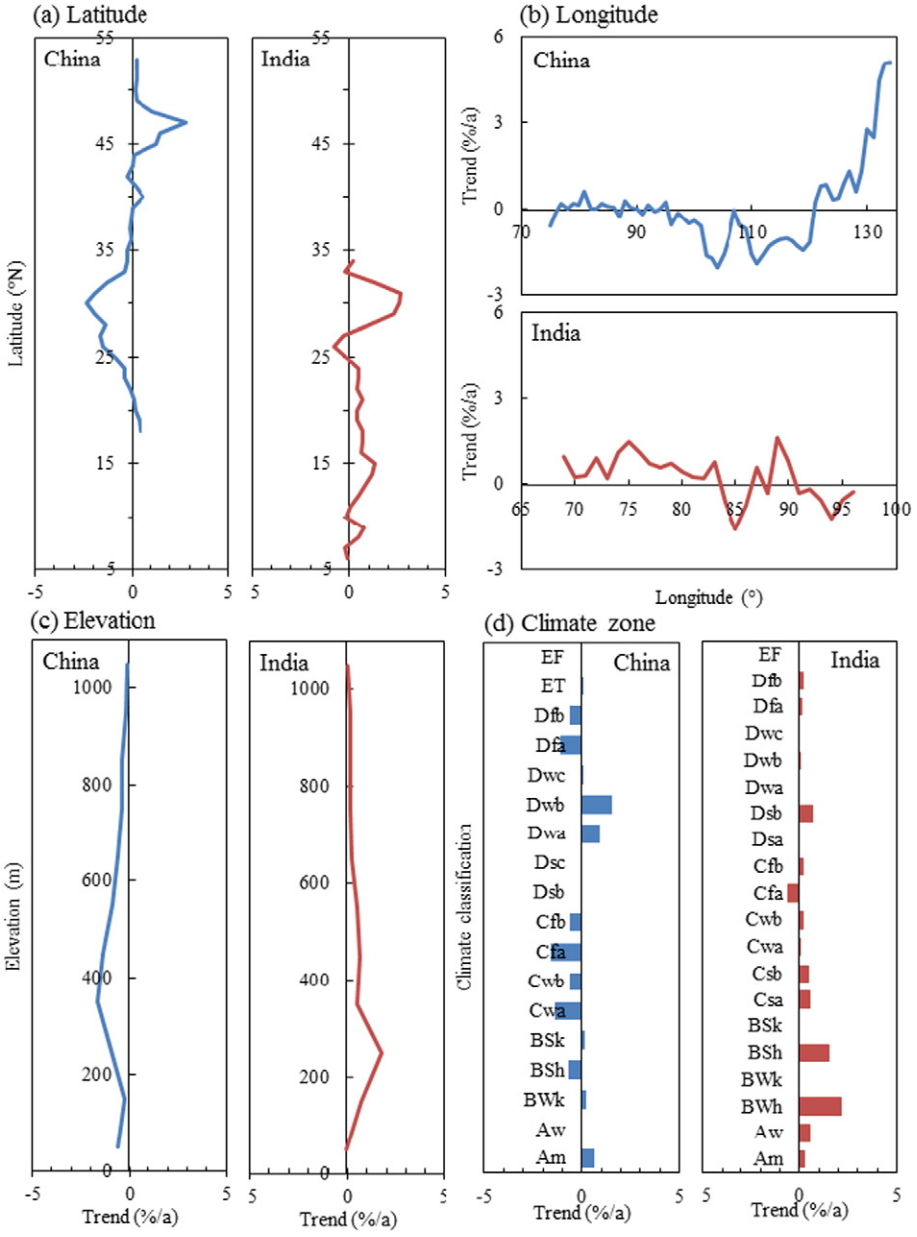


**Fig. 6.** Distribution of paddy rice change rates along different geographical gradients: (a) latitude gradients, (b) longitude gradients, (c) elevation gradients, and (d) climate zones. The climate zones are derived from the Köppen-Geiger climate classification (Peel et al., 2007). The meanings of codes in (d) can be found in Table S3. The distributions of different climate zones can be found in Fig. S6.

(Yu et al., 2013). In addition, some studies also integrated these existing cropland products to generate a new one with higher accuracy (e.g., IIASA-IFPRI) (Fritz et al., 2015). The aforementioned land cover data products treat cropland as one category, and therefore cannot support studies that seek to use crop specific data for food security, water resources use, greenhouse gas (GHG) emissions and climate. Currently, there are no global scale paddy rice maps derived from analyses of remote sensing images, let alone the temporal monitoring of the distribution of paddy rice fields.

Paddy rice mapping has been conducted at regional scales. For example, in USA, the Cropland Data Layer (CDL) is based on intensive sample data and supervised classification approach (Johnson and Mueller, 2010). In China, National Land Cover Datasets is based on labor intensive visual interpretation (Liu et al., 2005). However, these data products are not temporally continuous and cannot provide satellite evidence for the paddy rice variations in China, nor in India. A consistent, continuous, and robust paddy rice mapping strategy is needed to track spatiotemporal shifts in paddy rice fields in China and India. Using the RICE-MODIS platform, which combines time series MODIS-derived vegetation indices data and a phenology-based approach, we generated annual paddy rice maps for the two global leaders in paddy rice production. To our limited knowledge, these are the first annual national-scale products for either China or India over the previous 16 years. The maps produced by this study will be available in the Earth Observation and Modeling Facility (EOMF) data portal (http://www.eomf.ou.edu/) of the University of Oklahoma, and are expected to provide valuable information regarding a number of food security and environmental issues.

### *4.2. Annual maps of paddy rice planting area at 500-m spatial resolution in China and India*

Through spatiotemporal analyses of these annual maps of paddy rice planting area, we found that China experienced a significant northward

shift in the paddy rice field distribution characterized as a decrease in southern China and an increase in northern China, while India had an increase in the whole paddy rice planting area. Our results in China were consistent with the findings from previous studies about the shift in spatiotemporal distribution of paddy rice fields (Li et al., 2015; Liu et al., 2013; Piao et al., 2010), that is, a significant expansion of paddy rice fields in northern China and decrease in southern China. Several studies at regional scales also reported regional changes in paddy rice field distribution in China. For example, paddy rice fields have expanded in the wetlands of northeastern China, especially the Sanjiang Plain of Heilongjiang Province (Liu et al., 2004; Shi et al., 2013; Wang et al., 2011; Yang et al., 2007; Zhang et al., 2009).

Our conclusions are also supported by the studies based on different approaches. For example, Liu et al. (2013) generated spatial distributions of rice area and production results by using the Spatial Production Allocation Model (SPAM) and a series of datasets including cropland distribution, agricultural census data, agricultural irrigation data, and crop suitability data. The results showed a northeast shift of the paddy rice centroid in China. Through analyses of cropland census data, Cheng et al. (2012) also found a northward shift in the paddy rice pattern. In India, there were few works on changes in the distribution of paddy rice fields at regional or subnational scales (Gumma et al., 2015; Rao and Rao, 1987).

Although agricultural census data can track the annual variations of paddy rice area at regional or national scales (Tong et al., 2003), it cannot show where the paddy rice changes occurred. Moreover, the officially agricultural census data of China cannot effectively track the variations of paddy rice area; many studies have mentioned that census data in China could be biased due to political and policy factors (Frolking et al., 1999; Seto et al., 2000; Xiao et al., 2003). In addition, the planting areas of paddy rice derived from MODIS data in this study were not comparable to the sown areas from the agricultural census data. The annual maps of paddy rice planting area from this study provides spatiotemporally explicit information compared to the existing results from model simulations and agricultural census data.

### *4.3. Drivers of paddy rice agriculture shifts in China and India and implications on food security*

What is driving the shifts in paddy rice distribution for each country? The answer is complex. In China, previous studies revealed that the market and technical advances were two major factors influencing the paddy rice planting area dynamics (Cheng et al., 2012). For example, in southern China, previous studies showed that the economic development, smaller size of paddy rice fields, and the low agriculture comparative benefit have accelerated the decrease of paddy rice planting area (Cheng et al., 2012; Xu et al., 2013). Our results showed an evident decrease in paddy rice fields in southern China from 2000 to 2015 (Fig. 5). One possible reason for the decrease is that urbanization, industrialization, and infrastructure development have replaced a lot of croplands. Another possible explanation is the lack of labor force for paddy rice planting as young farmers migrate to cities to pursue higher payment jobs. Conversely, in Northeast China, rice agriculture expanded largely due to the large-scale agricultural operations, especially the state-owned farms have better agricultural infrastructure. Our previous study also demonstrated that the market price of rice is one of the important drivers in Northeast China, which directly motivated the farmers' decisions of paddy rice planting (Dong et al., 2016). In India, rapid economic growth and improvement of infrastructure, including the increased capacity of irrigation across the country, may be one important reason for the increase in paddy rice fields (Hazell and Wood, 2008). Loss in paddy rice field area is expected to increase in the future as urban population growth continues (Pandey and Seto, 2015), especially in the two most populous countries—India and China.

In addition, climate change and variability will always be a critical concern and constraint factor for agriculture and food security in the future (Lobell et al., 2008). For example, the increase in climate-change driven drought events may further threaten paddy rice agriculture in southern China (Huang et al., 2014) and the whole India (admin, 2015; GALLUCCI, 2015). Li et al. (2015) found that climate change is one of the major driving forces for the rice relocation in China. In India, our results showed a slightly decreasing trend from 2013 to 2015, and the recent climate-change driven drought events have been widely considered as an important driver (admin, 2015; GALLUCCI, 2015).

Although the paddy rice planting area has decreased, rice production in China showed an increasing trend generally (Liu et al., 2013). In India, annual rice production is highly variable despite the increased rice planting area. One of the reasons could be that the irrigated rice dominates China's rice production while rain-fed rice accounts for a large proportion in India, which is vulnerable to climate variability.

### *4.4. Uncertainty analysis and future development in paddy rice mapping*

Although our annual maps of paddy rice planting areas are consistent with existing products and have reasonably high accuracy, mapping paddy rice in tropical humid areas could still be a difficult task due to a few reasons.

First, the lack of cloud-free observations over the year prohibits analyses. Fig. S10 demonstrates the cloud frequency among all observations within a year. The tropical regions have more dense cloud coverage than in the mid-latitude areas. Moreover, due to the monsoonal climate, flooding signals of paddy rice fields are obscured from detection from early June to August (Fig. S11). As a result, analysis of optical images in tropical regions results in a higher omission error.

Second, the uncertainty of the paddy rice maps could be from the coarse spatial resolution of MODIS (Jain et al., 2013), as 500-m MODIS pixels could contain several land cover types or different crops within a pixel. The mixed pixels occur widely in mountainous areas, such as the montane regions of southern China (Fig. S12). Likewise, small-scale fields with different crops in close proximity to each other contribute to the mixed pixel issue, which will also weaken the flooding signal of paddy rice. Mixed pixel issues are expected to be solved in the future through application of images with finer spatial resolutions, such as Landsat. Several recent studies have reported that the time series Landsat images can be used to detect changes in paddy rice fields in temperate climate regions (Dong et al., 2015; Qin et al., 2015; Zhou et al., 2016). However, Landsat's utility in tropical regions is still unknown due to more clouds, longer revisit period, and multiple crops in a year. The recently launched Sentinel-2A is expected to provide higher temporal resolution images with 10-m resolution (Drusch et al., 2012). The improved Sentinel-2A data, in combination with Landsat data, may enable the algorithm to be feasible for monitoring paddy rice fields at a spatial resolution of 30-m in the future. Another promising method is the analysis of cloud-free SAR data. For example, SAR satellite images have been used for paddy rice mapping at demonstration sites across Asia in the RIICE project (Nelson et al., 2014); integrated SAR with optical satellite images have also been used for rice area monitoring in Mekong Delta, Vietnam (Karila et al., 2014). However, continuous monitoring at larger scales is still challenging due to the SAR data availability. Due to poor observations for MODIS data in tropical regions of study area, cropping intensity (e.g., single, double cropping) was not examined in this study but will be considered in our future study.

## 5. Conclusions

This study provides an analysis of inter-annual variations and changes in paddy rice cultivation at large, landscape scales for the two most populous countries, China and India. We showed a remarkable expansion in northeastern China and decrease in southern China, along with expansion across almost the whole country in India from 2000 to 2015. To our limited knowledge, this study provides the first annual

paddy rice maps for China and India based upon the hyper-temporal MODIS imagery and a phenology-based algorithm (RICE-MODIS). The potential to apply our novel algorithm to Landsat data is still unclear, especially in the humid tropical region where useful observations are scarce. However, the increasing data availability through coupling Sentinel-2A/B with Landsat 8 data will definitely contribute to finer resolution paddy rice mapping.

These annual paddy rice maps produced by this study provide an opportunity to study in greater detail methane emission estimation, food security, water resource use, and other relevant issues that are critical for the global food security and human wellbeing. While this study focused on changes in paddy rice agriculture at the national level, more studies are needed to understand the mechanisms and their regional differences in both China and India. Further research is encouraged; of particular interest are the drivers of paddy rice field expansion in high latitude areas and the abandonment of fields in tropical regions.

## Acknowledgements

This study was supported by research grants from the NASA Land Use and Land Cover Change program (NNX11AJ35G and NNX14AD78G) and the National Institutes of Health (NIH) NIAID (1R01AI101028-01A2). We thank Brian Alikhani for his comments in the earlier versions.

## Appendix A. Supplementary data

Supplementary data to this article can be found online at http://dx.doi.org/10.1016/j.scitotenv.2016.10.223.

## References

admin, 2015. Planting of main paddy rice crop of India 2015–16 (Kharif) slows down as it is near completion. 2015, riceoutlook. http://riceoutlook.com/planting-of-main-paddy-rice-crop-of-india-2015-16kharif-slows-down-as-it-is-near-completion/ .

Arino, O., Bicheron, P., Achard, F., Latham, J., Witt, R., Weber, J.L., 2008. GLOBCOVER the Most Detailed Portrait of Earth. Esa Bulletin-European Space Agency. pp. 24–31.

Biradar, C.M., Xiao, X.M., 2011. Quantifying the area and spatial distribution of double- and triple-cropping croplands in India with multi-temporal MODIS imagery in 2005. Int. J. Remote Sens. 32, 367–386.

Bouvet, A., Le Toan, T., Nguyen, L.-D., 2009. Monitoring of the rice cropping system in the Mekong Delta using ENVISAT/ASAR dual polarization data. IEEE Trans. Geosci. Remote Sens. 47, 517–526.

Chen, H., Zhu, Q.A., Peng, C.H., Wu, N., Wang, Y.F., Fang, X.Q., et al., 2013. Methane emissions from rice paddies natural wetlands, lakes in China: synthesis new estimate. Glob. Chang. Biol. 19, 19–32.

Cheng, Y.-X., Wang, X.-Z., Guo, J.-P., Zhao, Y.-X., Huang, J.-F., 2012. The temporal-spatial dynamic analysis of China rice production. Sci. Agric. Sin. 45, 3473–3485.

Dong, Y.F., Sun, G.Q., Pang, Y., 2006. Monitoring of rice crop using ENVISAT ASAR data. Sci. China Ser. D Earth Sci. 49, 755–763.

Dong, J., Xiao, X., Kou, W., Qin, Y., Zhang, G., Li, L., et al., 2015. Tracking the dynamics of paddy rice planting area in 1986–2010 through time series Landsat images and phenology-based algorithms. Remote Sens. Environ. 162, 154–168.

Dong, J., Xiao, X., Zhang, G., Menarguez, M.A., Choi, C.Y., Qin, Y., et al., 2016. Northward expansion of paddy rice in northeastern Asia during 2000–2014. Geophys. Res. Lett. 43, 3754–3761.

Drusch, M., Del Bello, U., Carlier, S., Colin, O., Fernandez, V., Gascon, F., et al., 2012. Sentinel-2: ESA's optical high-resolution mission for GMES operational services. Remote Sens. Environ. 120, 25–36.

Friedl, M.A., Sulla-Menashe, D., Tan, B., Schneider, A., Ramankutty, N., Sibley, A., et al., 2010. MODIS collection 5 global land cover: algorithm refinements and characterization of new datasets. Remote Sens. Environ. 114, 168–182.

Fritz, S., See, L., McCallum, I., You, L., Bun, A., Moltchanova, E., et al., 2015. Mapping global cropland and field size. Glob. Chang. Biol. 21, 1980–1992.

Frolking, S., Xiao, X.M., Zhuang, Y.H., Salas, W., Li, C.S., 1999. Agricultural land-use in China: a comparison of area estimates from ground-based census and satellite-borne remote sensing. Glob. Ecol. Biogeogr. 8, 407–416.

Frolking, S., Qiu, J.J., Boles, S., Xiao, X.M., Liu, J.Y., Zhuang, Y.H., et al., 2002. Combining remote sensing and ground census data to develop new maps of the distribution of rice agriculture in China. Glob. Biogeochem. Cycles 16.

Frolking, S., Yeluripati, J.B., Douglas, E., 2006. New district-level maps of rice cropping in India: a foundation for scientific input into policy assessment. Field Crop Res. 98, 164–177.

Gallucci, M., 2015. India drought 2015: climate change is biggest threat to India's economy, modi finance aide says, International Business Times. http://www.ibtimes.com/india-drought-2015-climate-change-biggest-threat-indias-economy-modi-finance-aide-2165051.

Gilbert, M., Xiao, X.M., Pfeiffer, D.U., Epprecht, M., Boles, S., Czarnecki, C., et al., 2008. Mapping H5N1 highly pathogenic avian influenza risk in Southeast Asia. Proc. Natl. Acad. Sci. U. S. A. 105, 4769–4774.

Gilbert, M., Golding, N., Zhou, H., Wint, G.R.W., Robinson, T.P., Tatem, A.J., et al., 2014. Predicting the risk of avian influenza A H7N9 infection in live-poultry markets across Asia. Nat. Commun. 5.

Gumma, M.K., Nelson, A., Thenkabail, P.S., Singh, A.N., 2011. Mapping rice areas of South Asia using MODIS multitemporal data. J. Appl. Remote. Sens. 5, 053547.

Gumma, M.K., Thenkabail, P.S., Maunahan, A., Islam, S., Nelson, A., 2014. Mapping seasonal rice cropland extent and area in the high cropping intensity environment of Bangladesh using MODIS 500 m data for the year 2010. ISPRS J. Photogramm. Remote Sens. 91, 98–113.

Gumma, M.K., Mohanty, S., Nelson, A., Arnel, R., Mohammed, I.A., Das, S.R., 2015. Remote sensing based change analysis of rice environments in Odisha, India. J. Environ. Manag. 148, 31–41.

Hall, D.K., Riggs, G.A., Salomonson, V.V., 1995. Development of methods for mapping global snow cover using moderate resolution imaging spectroradiometer data. Remote Sens. Environ. 54, 127–140.

Hall, D.K., Riggs, G.A., Salomonson, V.V., DiGirolamo, N.E., Bayr, K.J., 2002. MODIS snow-cover products. Remote Sens. Environ. 83, 181–194.

Hazell, P., Wood, S., 2008. Drivers of change in global agriculture. Philos. Trans. R. Soc., B 363, 495–515.

Huang, W., Sui, Y., Yang, X., Dai, Z., Qu, H., Li, M., 2014. Spatio-temporal characteristics of crop drought in southern China based on drought index of continuous days without available precipitation. Trans. Chin. Soc. Agric. Eng. 30, 125–135.

Huete, A., Didan, K., Miura, T., Rodriguez, E.P., Gao, X., Ferreira, L.G., 2002. Overview of the radiometric and biophysical performance of the MODIS vegetation indices. Remote Sens. Environ. 83, 195–213.

Jain, M., Mondal, P., DeFries, R.S., Small, C., Galford, G.L., 2013. Mapping cropping intensity of smallholder farms: a comparison of methods using multiple sensors. Remote Sens. Environ. 134, 210–223.

Jin, C., Xiao, X., Dong, J., Qin, Y., Wang, Z., 2015. Mapping paddy rice distribution using multi-temporal Landsat imagery in the Sanjiang Plain, northeast China. Front. Earth Sci. 1-14.

Shi, J.-j., J-f, H., Zhang, F., 2013. Multi-year monitoring of paddy rice planting area in Northeast China using MODIS time series data. J. Zheijang Univ. Sci. B 14, 934–946.

Johnson, D.M., Mueller, R., 2010. The 2009 cropland data layer. Photogramm. Eng. Remote. Sens. 76, 1201–1205.

Karila, K., Nevalainen, O., Krooks, A., Karjalainen, M., Kaasalainen, S., 2014. Monitoring changes in rice cultivated Area from SAR and optical satellite images in Ben Tre and Tra Vinh Provinces in Mekong Delta, Vietnam. Remote Sens. 6, 4090–4108.

Kontgis, C., Schneider, A., Ozdogan, M., 2015. Mapping rice paddy extent and intensification in the Vietnamese Mekong River Delta with dense time stacks of Landsat data. Remote Sens. Environ. 169, 255–269.

Kuenzer, C., Knauer, K., 2013. Remote sensing of rice crop areas. Int. J. Remote Sens. 34, 2101–2139.

Li, C., Xiao, X., Frolking, S., Moore, B., Salas, W., Qiu, J., et al., 2003. Greenhouse gas emissions from croplands of China. J. Quat. Sci. 23, 493–503.

Li, Z.G., Liu, Z.H., Anderson, W., Yang, P., Wu, W.B., Tang, H.J., et al., 2015. Chinese rice production area adaptations to climate changes, 1949-2010. Environ. Sci. Technol. 49, 2032–2037.

Liu, H.Y., Zhang, S.K., Li, Z.F., Lu, X.G., Yang, Q., 2004. Impacts on wetlands of large-scale land-use changes by agricultural development: the small Sanjiang Plain, China. Ambio 33, 306–310.

Liu, J., Liu, M., Tian, H., Zhuang, D., Zhang, Z., Zhang, W., et al., 2005. Spatial and temporal patterns of China's cropland during 1990–2000: an analysis based on Landsat TM data. Remote Sens. Environ. 98, 442–456.

Liu, J.Y., Zhang, Z.X., Xu, X.L., Kuang, W.H., Zhou, W.C., Zhang, S.W., et al., 2010. Spatial patterns and driving forces of land use change in China during the early 21st century. J. Geogr. Sci. 20, 483–494.

Liu, Z., Li, Z., Tang, P., Li, Z., Wu, W., Yang, P., et al., 2013. Change analysis of rice area and production in China during the past three decades. J. Geogr. Sci. 23, 1005–1018.

Liu, J., Kuang, W., Zhang, Z., Xu, X., Qin, Y., Ning, J., et al., 2014a. Spatiotemporal characteristics, patterns, and causes of land-use changes in China since the late 1980s. J. Geogr. Sci. 24, 195–210.

Liu, Z., Yang, P., Tang, H., Wu, W., Zhang, L., Yu, Q., et al., 2014b. Shifts in the extent and location of rice cropping areas match the climate change pattern in China during 1980–2010. Reg. Environ. Chang. 15, 919–929.

Lobell, D.B., Burke, M.B., Tebaldi, C., Mastrandrea, M.D., Falcon, W.P., Naylor, R.L., 2008. Prioritizing climate change adaptation needs for food security in 2030. Science 319, 607–610.

Maclean, J.L., Hettel, G.P., 2002. Rice Almanac: Source Book for the Most Important Economic Activity on Earth: IRRI (Free PDF Download) .

Miyaoka, K., Maki, M., Susaki, J., Homma, K., Noda, K., Oki, K., 2013. Rice-planted area mapping using small sets of multi-temporal SAR data. IEEE Geosci. Remote Sens. Lett. 1–5.

Nelson, A., Gumma, M.K., 2015. In: IRRI (Ed.), A Map of Lowland Rice Extent in the Major Rice Growing Countries of Asia. IRRI, Los Banos, Philippines .

Nelson, A., Setiyono, T., Rala, A.B., Quicho, E.D., Raviz, J.V., Abonete, P.J., et al., 2014. Towards an operational SAR-based rice monitoring system in Asia: examples from 13 demonstration sites across Asia in the RIICE project. Remote Sens. 6, 10773–10812.

Pandey, B., Seto, K.C., 2015. Urbanization and agricultural land loss in India: comparing satellite estimates with census data. J. Environ. Manag. 148, 53–66.

Peel, M., Finlayson, B., McMahon, T., 2007. Updated world map of the Koppen-Geiger climate classification. Hydrol. Earth Syst. Sci. 11, 1633–1644.

Piao, S.L., Ciais, P., Huang, Y., Shen, Z.H., Peng, S.S., Li, J.S., et al., 2010. The impacts of climate change on water resources and agriculture in China. Nature 467, 43–51.
Qin, Y., Xiao, X., Dong, J., Zhou, Y., Zhu, Z., Zhang, G., et al., 2015. Mapping paddy rice planting area in cold temperate climate region through analysis of time series Landsat 8 (OLI), Landsat 7 (ETM+) and MODIS imagery. ISPRS J. Photogramm. Remote Sens. 105, 220–233.
Qin, Y., Xiao, X., Dong, J., Zhang, G., Roy, P.S., Joshi, P.K., et al., 2016. Mapping forests in monsoon Asia with ALOS PALSAR 50-m mosaic images and MODIS imagery in 2010. Sci. Report. 6, 20880.
Rao, P.P.N., Rao, V.R., 1987. Rice crop identification and area estimation using remotely-sensed data from Indian cropping patterns. Int. J. Remote Sens. 8, 639–650.
Sakamoto, T., Van Phung, C., Kotera, A., Nguyen, K.D., Yokozawa, M., 2009. Analysis of rapid expansion of inland aquaculture and triple rice-cropping areas in a coastal area of the Vietnamese Mekong Delta using MODIS time-series imagery. Landsc. Urban Plan. 92, 34–46.
Samad, M., Merrey, D., Vermillion, D., Fuchscarsch, M., Mohtadullah, K., Lenton, R., 1992. Irrigation management strategies for improving the performance of irrigated agriculture. Outlook Agric. 21, 279–286.
Sass, R.L., Cicerone, R.J., 2002. Photosynthate allocations in rice plants: food production or atmospheric methane? Proc. Natl. Acad. Sci. U. S. A. 99, 11993–11995.
Seto, K.C., Kaufmann, R.K., Woodcock, C.E., 2000. Landsat reveals China's farmland reserves, but they're vanishing fast. Nature 406, 121.
Sun, H.S., Huang, J.F., Huete, A.R., Peng, D.L., Zhang, F., 2009. Mapping paddy rice with multi-date moderate-resolution imaging spectroradiometer (MODIS) data in China. J. Zhejiang Univ. Sci. A 10, 1509–1522.
Tong, C.L., Hall, C.A.S., Wang, H.Q., 2003. Land use change in rice, wheat and maize production in China (1961-1998). Agric. Ecosyst. Environ. 95, 523–536.
van Groenigen, K.J., van Kessel, C., Hungate, B.A., 2013. Increased greenhouse-gas intensity of rice production under future atmospheric conditions. Nat. Clim. Chang. 3, 288–291.
Vermote, E., Vermeulen, A., 1999. Atmospheric Correction Algorithm: Spectral Reflectances (MOD09). ATBD Version. 4.
Wang, Z.M., Song, K.S., Ma, W.H., Ren, C.Y., Zhang, B., Liu, D.W., et al., 2011. Loss and fragmentation of marshes in the Sanjiang Plain, Northeast China, 1954–2005. Wetlands 31, 945–954.
Wang, J., Xiao, X., Qin, Y., Dong, J., Zhang, G., Kou, W., et al., 2015. Mapping paddy rice planting area in wheat-rice double-cropped areas through integration of Landsat-8 OLI, MODIS, and PALSAR images. Sci. Report. 5, 10088.
Wu, F., Wang, C., Zhang, H., Zhang, B., Tang, Y.X., 2011. Rice crop monitoring in South China with RADARSAT-2 quad-polarization SAR data. IEEE Geosci. Remote Sens. Lett. 8, 196–200.
Xiao, X., Boles, S., Frolking, S., Salas, W., Moore, B., Li, C., et al., 2002a. Landscape-scale characterization of cropland in China using vegetation and landsat TM images. Int. J. Remote Sens. 23, 3579–3594.
Xiao, X., Boles, S., Frolking, S., Salas, W., Moore, B., Li, C., et al., 2002b. Observation of flooding and rice transplanting of paddy rice fields at the site to landscape scales in China using VEGETATION sensor data. Int. J. Remote Sens. 23, 3009–3022.
Xiao, X., Boles, S., Liu, J., Zhuang, D., Liu, M., 2002c. Characterization of forest types in Northeastern China, using multi-temporal SPOT-4 VEGETATION sensor data. Remote Sens. Environ. 82, 335–348.
Xiao, X.M., Liu, J.Y., Zhuang, D.F., Frolking, S., Boles, S., Xu, B., et al., 2003. Uncertainties in estimates of cropland area in China: a comparison between an AVHRR-derived dataset and a Landsat TM-derived dataset. Glob. Planet. Chang. 37, 297–306.
Xiao, X.M., Boles, S., Liu, J.Y., Zhuang, D.F., Frolking, S., Li, C.S., et al., 2005. Mapping paddy rice agriculture in southern China using multi-temporal MODIS images. Remote Sens. Environ. 95, 480–492.
Xiao, X., Boles, S., Frolking, S., Li, C., Babu, J.Y., Salas, W., et al., 2006. Mapping paddy rice agriculture in South and Southeast Asia using multi-temporal MODIS images. Remote Sens. Environ. 100, 95–113.
Xiao, X., Biradar, C., Czarnecki, C., Alabi, T., Keller, M., 2009. A simple algorithm for large-scale mapping of evergreen forests in tropical America, Africa and Asia. Remote Sens. 1, 355–374.
Xu, C., Sun, L., Zhou, X., Li, F., Fang, F., 2013. Characteristics of rice production in South China and policy proposals for its steady development. Res. Agric. Mod. 34, 129–132.
Yang, X., Lin, E., Ma, S.M., Ju, H., Guo, L.P., Xiong, W., et al., 2007. Adaptation of agriculture to warming in Northeast China. Clim. Chang. 84, 45–58.
Yang, S.B., Shen, S.H., Li, B.B., Le Toan, T., He, W., 2008. Rice mapping and monitoring using ENVISAT ASAR data. IEEE Geosci. Remote Sens. Lett. 5, 108–112.
Yu, L., Wang, J., Clinton, N., Xin, Q.C., Zhong, L.H., Chen, Y.L., et al., 2013. FROM-GC: 30 m global cropland extent derived through multisource data integration. Int. J. Digital Earth 6, 521–533.
Zhang, S.Q., Na, X.D., Kong, B., Wang, Z.M., Jiang, H.X., Yu, H., et al., 2009. Identifying wetland change in China's Sanjiang Plain using remote sensing. Wetlands 29, 302–313.
Zhang, G., Xiao, X., Dong, J., Kou, W., Jin, C., Qin, Y., et al., 2015. Mapping paddy rice planting areas through time series analysis of MODIS land surface temperature and vegetation index data. ISPRS J. Photogramm. Remote Sens. 106, 157–171.
Zhou, Y., Xiao, X., Qin, Y., Dong, J., Zhang, G., Kou, W., et al., 2016. Mapping paddy rice planting area in rice-wetland coexistent areas through analysis of Landsat 8 OLI and MODIS images. Int. J. Appl. Earth Obs. Geoinf. 46, 1–12.
Zuo, L., Zhang, Z., Zhao, X., Wang, X., Wu, W., Yi, L., et al., 2014. Multitemporal analysis of cropland transition in a climate-sensitive area: a case study of the arid and semiarid region of northwest China. Reg. Environ. Chang. 14, 75–89.